Bulletin of Earthquake Engineering (2024) 22:159–189
https://doi.org/10.1007/s10518-023-01668-0

S.I. : NATECH RISK ASSESSMENT OF HAZARDOUS FACILITIES

Do soft soil layers reduce the seismic kinematic distress of onshore high-pressure gas pipelines?

Nikolaos Makrakis[1] · Prodromos N. Psarropoulos[2] · Anastasios Sextos[3] · Yiannis Tsompanakis[1]

Received: 3 September 2022 / Accepted: 5 March 2023 / Published online: 3 May 2023

Abstract
Onshore high-pressure gas pipelines constitute critical infrastructure that usually cross seismic-prone regions and are vulnerable to Permanent Ground Deformations (PGDs) due to active seismic faults. In design, it may not be feasible to avoid fault rupture areas due to various technical, economical and topographic reasons. Moreover, the presence of soil layers affects the PGDs resulting from a tectonic fault, which in turn may alter the seismic demand on the pipeline. The current study investigates numerically the impact of soft soil layers on the seismic kinematic distress of onshore gas pipelines. For this purpose, a decoupled numerical modeling approach is adopted, consisting of two separate finite-element models for the simulation of soil response and pipeline distress, respectively. Soil non-linearities are taken into account utilizing the Mohr-Coulomb constitutive model with isotropic strain softening. An extensive parametric analysis is performed considering different faulting mechanisms and fault dip angles, as well as soil geometry and mechanical properties. Consequently, the maximum absolute values of both tensile and compressive pipeline strains are correlated with the seismic intensity level (i.e., in terms of bedrock offset which is associated with earthquake magnitude via simple relationships). The paper concludes with a set of design charts and tables for the preliminary seismic design of onshore high-pressure gas pipelines. These charts and tables predict with reasonable accuracy pipeline deformations, in terms of strains, for different magnitude, fault type, dip angle, sand type, and varying overlying soil layer thickness.

Keywords Gas pipelines · Seismic faulting · Fault rupture propagation · Permanent ground deformations · Sandy deposits · Finite-element method

1 Introduction

Large-scale infrastructure, such as gas pipelines, constitute crucial energy facilities that often cross extensive seismic-prone areas. In general, earthquakes can cause severe damages to above-ground structures and infrastructure due to the inertial distress caused

✉ Yiannis Tsompanakis
jt@science.tuc.gr

Extended author information available on the last page of the article

by strong ground shaking and/or due to the kinematic distress caused by permanent ground deformations (PGDs). On the other hand, buried natural gas pipelines can be distressed kinematically, apart from PGDs, from transient ground deformations (TGDs) as well, while buried pipelines transferring liquids (e.g., water, oil) can also be inertially distressed. TGDs can be detrimental for buried pipelines under certain local site conditions (e.g., Psyrras et al. 2018); however, the kinematic distress due to PGDs is more common and more adverse for all types of pipelines.

Earthquake-induced PGDs can broadly be defined as irreversible soil movement due to slope failure, soil liquefaction and lateral spreading, as well as tectonic faulting. High-pressure gas pipelines are considerably vulnerable to PGDs due to tectonic faulting, and consequently, several case studies have been reported demonstrating severe pipeline networks failures (Nair et al. 2018). Since avoiding fault rupture areas might not be feasible from a technical and/or economic perspective, the effect of fault rupture propagation to ground surface, in terms of PGDs, as well as the consequent kinematic distress of the pipeline, in terms of strains, have a significant practical importance, thus, highlighting the necessity for an accurate and reliable assessment of PGDs and pipeline seismic demand due to tectonic faulting.

Along these lines, the structural integrity of a pipeline subjected to fault rupture has extensively been investigated in the literature by means of analytical, numerical, and experimental methodologies. In particular, simplified analytical procedures were initially developed, due to the lack of suitable numerical software (Newmark and Hall 1975; Kennedy et al. 1977; Wang and Yeh 1985). Numerical methods have gradually evolved by taking into account the critical role of pipeline service loads, the non-linear behavior of the surrounding soil, as well as the pipe-soil interaction non-linearities (Karamitros et al. 2007, 2011; Trifonov and Cherniy 2012; Sarvanis and Karamanos 2017; Zhang et al. 2017). In addition, the impact of bends, which can highly influence the behavior of pipelines subjected to fault displacements has been investigated in a number of studies (e.g., Karamitros et al. 2016; Vazouras and Karamanos 2017).

The numerical studies are usually based on the finite element method (FEM), and fall into two categories, namely *coupled* and *decoupled*. According to the *coupled* approach, the pipeline, which is usually modeled using shell elements, and the surrounding soil (or rock) stratum, modeled with 3-D elements, are included in the same finite element (FE) model utilizing appropriate contact elements (Vazouras et al. 2015; Özcebe et al. 2017; Gawande et al. 2019; Dey et al. 2020). Although coupled finite-element based models are reliable for the extension of experimental results (Robert et al. 2016; Jalali et al. 2018; Tsatsis et al. 2019; Fadaee et al. 2020), their high computational demand makes extensive parametric investigations impractical and sensitive to FEM instabilities.

On the other hand, the *decoupled* approach is based on sub-structuring the physical problem into two separate FE models: one for the pipeline and one for the wider soil (or rock) stratum. It is worth noticing that the decoupled approach reasonably assumes free-field conditions for fault outcropping, since the stiffness of the pipeline is significantly smaller than the stiffness of the moving soil bed. Pipeline FE modeling is commonly carried out utilizing beam or pipe elements, whereas pipe —ground (i.e., soil or bedrock) interaction is simulated by means of bi-linear soil springs. Soil springs are utilized to impose the PGDs on the pipeline (Joshi et al. 2011; Uckan et al. 2015; Melissianos et al. 2016). Alternative hybrid methodologies have also been developed using beam and shell FE for the pipeline simulation (Xie et al. 2011) as well as solid block and spring elements for the surrounding soil bed (Halabian and Hokmabadi 2018) and surface-to-surface contact elements (Psyrras et al. 2018).

The experimental investigation of fault-pipe intersection is even more demanding compared to numerical and analytical approaches. Considerable research effort has been devoted on the performance of full-scale experiments, aiming to investigate the impact that crucial factors (e.g., pipe material roughness and embedment depth, surrounding soil density, fault offset, etc.) may have on the pipeline kinematic distress and pipe-soil interaction due to tectonic faulting (Yoshizaki et al. 2003; Rofooei et al. 2012; Jalali et al. 2016, 2018; Sarvanis et al. 2018; Psyrras et al. 2020). Small-scale physical (Demirci et al. 2018; Tsatsis et al. 2019) and centrifuge (Ha et al. 2008; Rojhani et al. 2012; Saiyar et al. 2016) tests as well, have gradually replaced the costly and space-demanding full-scale experiments.

The problem of pipeline-fault intersection is of outmost importance, and this is evidenced by the fact that several international guidelines and standards have been developed for the seismic design of pipelines. Specifically, ASCE guidelines (ASCE 1984) have adopted, early on, the analytical model proposed by Newmark and Hall (1975), in order to evaluate the performance of a pipeline subjected to strike-slip and dip-slip faulting. American Lifelines Alliance (ALA 2001) have further established pipe strain limits for onshore pipe-soil interaction and different loading scenarios, combining analytical and numerical methodologies. Finally, Eurocode 8 (EC8 - Part 4) (CEN 2006) has proposed several mitigation measures for safe fault-pipe intersection.

Nonetheless, most of the aforementioned studies have investigated the problem of pipe-fault intersection assuming, rather unrealistically, that the pipeline is laid directly on the ruptured bedrock (Fig. 1a), i.e., without taking into account the presence of soil layer(s) that usually exist between the pipeline and the bedrock (Fig. 1b). In fact, earthquake fault rupture is directly associated with abrupt displacements within the excessively stiff body of Earth's crust. Moreover, very often the rigid bedrock is covered by soil layer(s) ranging from tens to hundreds of meters, thus, these displacements propagate within such deposit(s)

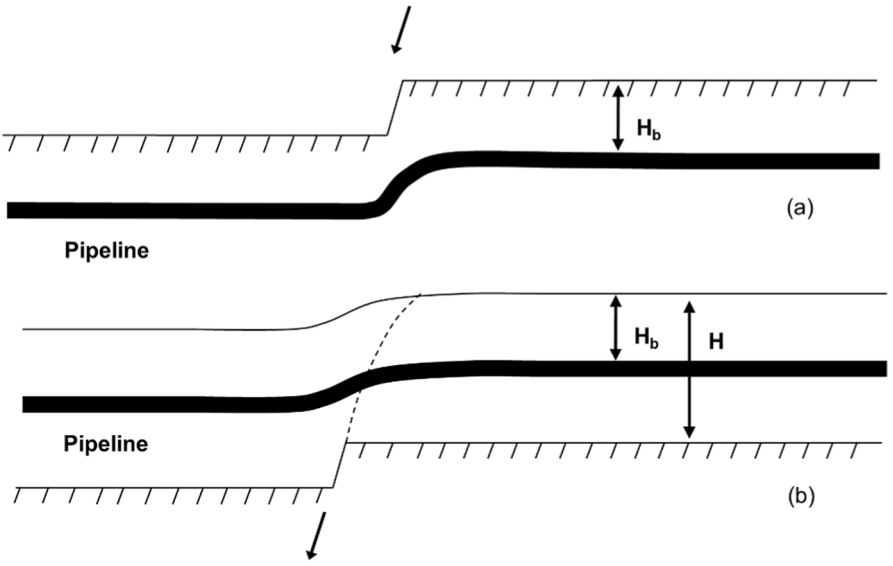

Fig. 1 Sketch showing a buried pipeline in the cases of: **a** rock—pipe interaction and **b** soil—pipe interaction. H_b is the depth of the buried pipeline, while H is the height of the soil layer

and may even reach the ground surface, forming shear failure zones. Consequently, fault rupture propagation and fault outcropping, which consist complex phenomena can affect the structural integrity of aboveground or buried facilities, such as gas pipelines.

Among the few studies that explored the impact of soil strata on buried pipelines that cross active seismic faults were the ones of Tsatsis et al. (2019) and Fadaee et al. (2020). In particular, Tsatsis et al. (2019) developed and experimentally verified a decoupled FE modeling approach to assess the behavior of a pipeline that is buried into a cohesionless soil cover and subjected to dip-slip faulting. Hence, a soil constitutive model with strain softening was utilized to simulate fault rupture propagation, whereas three-dimensional FE were chosen for the simulation of soil-pipe interaction. The work involved a parametric investigation considering several critical parameters (such as fault dip angle) that might affect pipeline's response, and subsequently, the relative outcomes reported their significant effect on pipe distress.

In the current study, the kinematic distress of such pipelines is evaluated taking into account the PGDs caused by both fault rupture propagation and fault outcropping. The main objective of the current paper, which is an extension of a recent conference paper (Makrakis et al. 2022a), is to correlate the earthquake magnitude, in terms of bedrock movement, with pipe distress, in terms of strains, considering the presence of soil layer that covers the rigid bedrock. This is achieved by means of extensive numerical analyses of a typical pipeline which is buried in a sandy soil deposit of varying thickness and mechanical properties, being subjected to dip-slip fault motion for different bedrock offset and dip angles. The results are summarized in the form of design charts and tables which can be applied in practice for the preliminary seismic design of onshore high-pressure gas pipelines.

2 Problem description

The first step for correlating seismic intensity to seismic demand on the pipe is to corelate earthquake magnitude with bedrock displacement utilizing well-established expressions. It is worth noticing that very few studies are available in the literature that analytically or empirically correlate the earthquake magnitude with characteristic tectonic parameters, such as bedrock displacement, either considering (Turgut et al. 2017) or ignoring (Chinnery 1969; Wells and Coppersmith 1994) the presence of overlying soil layer(s). In a companion paper of the current manuscript, new empirical relationships have been proposed for the assessment of the impact of sandy surface soil deposits on fault rupture propagation and the resulting soil surface inclination (Makrakis et al. 2023). In the current study the emphasis is given on deriving similar expressions to assess the kinematic distress of pipelines.

Wells and Coppersmith (1994) developed an extensive database consisting of more than 400 historical earthquake events and after a series of regression analyses, they empirically correlated tectonic parameters (e.g., average and maximum bedrock displacement) with earthquake magnitude. The relationship proposed by Wells and Coppersmith (1994) is adopted herein, where average bedrock displacement (AD) is related to earthquake moment magnitude M, according to the following logarithmic formula:

$$\log(AD) = a + b \cdot M \tag{1}$$

where α and b are regression coefficients equal to −4.80 and 0.69, with 0.36 standard deviation, and 0.57 and 0.08 standard errors, respectively. Note that Eq. (1) is valid for

M that ranges between 5.6 and 8.1 and AD from 0.05 to 8.0 m. It is also noteworthy that the present work, which is focused on the problem of fault-pipeline intersection, has considered the average bedrock displacement, rather than the maximum bedrock displacement, since AD describes the mean bedrock displacement observed along the fault rupture plane and it may affect a larger area of the pipeline.

It has to be stressed that the examined phenomenon is characterized by several complexities and uncertainties that cannot be fully covered by a Deterministic Seismic Hazard Analysis (DSHA), as the one described above. As presented in Eq. (1), this deterministic approach calculates the bedrock displacement with respect to earthquake magnitude and two regression coefficients. This postulates the occurrence of an earthquake of a specified magnitude at a specific location, which could affect the pipeline. However, DSHA does neither consider the earthquake occurrence probability nor the effect of uncertainties. Hence, it does not provide information regarding the expected magnitude of fault displacement within the lifespan of the pipeline. To overcome this deficiency, probabilistic fault displacement hazard analysis (PFDHA) can be adopted, as presented in recent studies (Melissianos et al. 2022; Melissianos 2022). PFDHA would be a very useful basis for further investigation and extension of the present work.

3 Numerical simulation

3.1 Analysis of soil response

Soil behavior due to fault rupture, fault rupture propagation and fault outcropping have been numerically simulated in a realistic manner by means of the Dynamic-Explicit analysis module of ABAQUS FE software (Simulia 2014). This module is commonly utilized to solve a wide range of quasi-static problems in a computationally efficient manner, without leading to convergence difficulties. However, for reliable pseudo-static results, the loading rates should be carefully selected, as inertia effects play a detrimental role in dynamic analyses. Hence, the current study has adopted the suggestions of Ni et al. (2018), where the maximum kinetic energy of the FE model should range between 5 and 10% of the total energy.

Figure 2 presents the 2D idealization of the developed numerical model. Particularly, rigid bedrock, which is located at the bottom of the FE model, is covered from a uniform soil layer of thickness H. After a comprehensive sensitivity analysis, the width of the FE model, B, has been chosen 4 or 8 times larger than H, in order to minimize undesired boundary effects. This approach has widely been adopted from several authors, who investigated the phenomenon of dip-slip fault rupture propagation (e.g., Bray 1990; Anastasopoulos et al. 2007; Rokonuzzaman et al. 2015).

Soil layer has been simulated in 2D plane-strain conditions utilizing the four-node quadrilateral elements (type CPE4). For the optimal numerical performance, a coarser FE mesh discretization has been used at the edges of the model, whereas a finer FE mesh has been selected near the failure plane, according to the suggestions of several studies (e.g., Anastasopoulos et al. 2007; Rokonuzzaman et al. 2015; Loli et al. 2018; Thebian et al. 2018; Mortazavi Zanjani and Soroush 2019). Figure 2 illustrates the FE model of thickness H = 20 m, where elements with dimensions 0.5 m x 0.5 m (width x height) and 1 m x 0.5 m have been used for the fine and coarse part of the FE mesh, respectively.

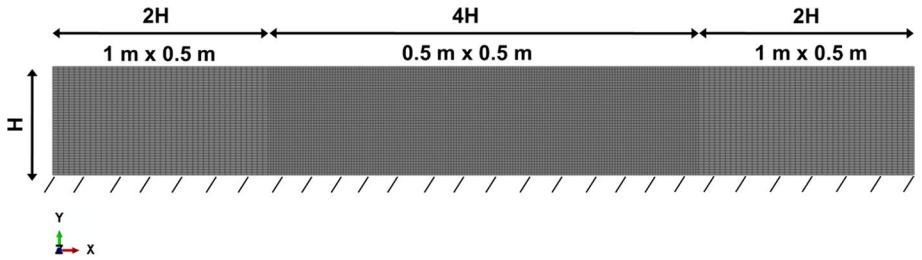

Fig. 2 Geometry and mesh discretization of a 20 m - thick soil deposit

Two steps have been created to carry out the numerical analyses, namely geostatic and fault displacement. More specifically, gravity force is applied in the FE model during the geostatic step. During the fault displacement step, bedrock dislocation (i.e., fault offset) is simulated in terms of a differential displacement at an angle α (i.e., fault dip angle) parallel to the fault plane. The left vertical side of the FE model and left bottom nodes move parallel to the fault plane according to the level of bedrock dislocation, thus representing the hanging wall of the fault. Oppositely, the right bottom nodes, which are fixed, and the right vertical side of the FE model, where roller boundary conditions have been imposed, represent the foot wall. Figure 3a and b display these loading and boundary conditions for the case of normal and reverse faulting, respectively.

3.1.1 Soil constitutive model

Significant research has been conducted on the non - linear response of soils in relation to fault crossing. Bray et al. (1994) and Scott (1987) concluded that soil non - linearities due to fault rupture are realistically captured accounting for the soil strain softening. Hence, several constitutive models have gradually been developed considering the non - linear soil stress - strain relationship. The current study adopted the elastoplastic Mohr - Coulomb constitutive model with isotropic strain softening, as introduced by Anastasopoulos et al. (2007).

In particular, the pre - yield soil behavior is defined in terms of the secant shear modulus, G, and is assumed to be elastic, whereas post - peak soil response is effectively captured via the Mohr - Coulomb failure criterion. An isotropic strain softening law is applied, where the mobilized friction and dilation angles are linearly decreased as the octahedral plastic shear strain, denoted as γ^{p}_{oct}, increases. Equations (2) to (5) describe the adopted constitutive model:

$$\varphi = \begin{cases} \varphi_p = \frac{\varphi_p - \varphi_{res}}{\gamma^p_f}\gamma^p_{oct} & for\ 0 \le \gamma^p_{oct} < \gamma^p_f \quad (2) \\ \varphi_{res} & for\ \gamma^p_{oct} \ge \gamma^p_f \quad (3) \end{cases}$$

$$\psi = \begin{cases} \psi_p = \left(1 - \frac{\gamma^p_{oct}}{\gamma^p_f}\right) & for\ 0 \le \gamma^p_{oct} < \gamma^p_f \quad (4) \\ \psi_{res} & for\ \gamma^p_{oct} \ge \gamma^p_f \quad (5) \end{cases}$$

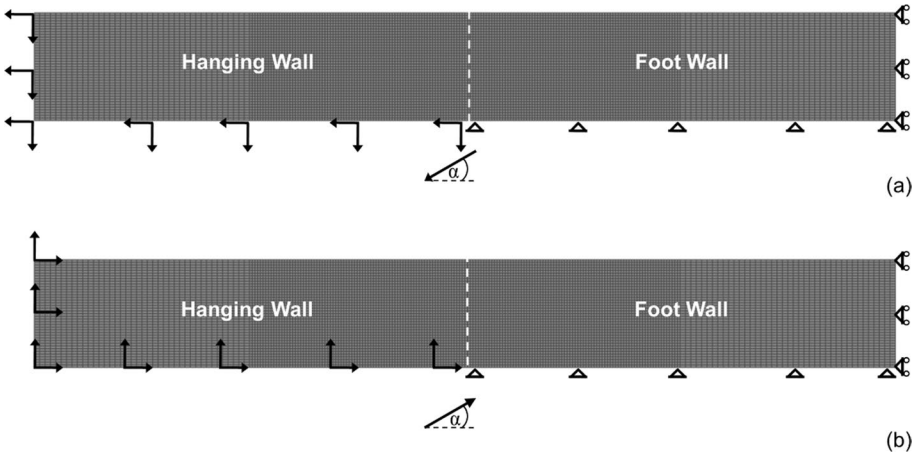

Fig. 3 Boundary and loading conditions for a 20 m - thick soil deposit for: **a** normal fault and **b** reverse fault

where, φ and ψ denote the friction and dilation angles, respectively. Moreover, φ_p and φ_{res} represent the ultimate mobilized (peak) and residual friction angles, respectively, whereas ψ_p and ψ_{res} denote the corresponding dilation angles. In addition, $\gamma^p{}_f$ describes the failure plastic octahedral shear strain at the end of strain softening. It should be noted that this soil constitutive model has been applied in ABAQUS FE software via a subroutine, which has been developed by authors' group (Chatzidakis et al. 2022).

Note that failure plastic octahedral shear strain at the end of strain softening is sensitive to scale effects, which necessitates to a careful selection of the FE size, d_{FE}. In general, the FE size should be equal to the shear band thickness, d_B. However, the fact that d_B is of the order of millimeters leads to unfeasible FE modeling (in terms of computational cost), especially in cases of large - scale problems. Hence, to overcome this problem, the d_{FE} / d_B ratio has been set equal to the ratio of the real shear strain over the FE - computed shear strain, as proposed by Anastasopoulos et al. (2007).

3.1.2 Experimental validation

The reliability and accuracy of the developed FE model have been verified by a 100 g centrifuge test that was conducted by Anastasopoulos et al. (2007). More specifically, a soil layer of thickness, H = 25 m, consisting of medium - dense Fontainebleau sand with relative density D_r = 80%, was subjected to dip - slip faulting with dip angle $\alpha = 60^o$. A wide range of bedrock dislocation, h, was examined equal to 0.25, 0.5, 0.85, 1.08 m and 0.18, 0.49, 0.7, 1.13 m regarding normal and reverse fault, respectively.

The corresponding numerical results, which were compared to the experimental ones in terms of ground - surface vertical displacements, dz, revealed a good agreement between numerical and experimental methodologies, for low levels of vertical bedrock dislocation, regardless of fault type. However, slightly different ground surface displacements were observed for larger fault offset. Hence, the proposed FE, in conjunction with the previously described soil constitutive model, can be successfully used to investigate the phenomena of fault rupture and fault outcropping. It should be mentioned that a detailed presentation of the numerical model and the corresponding results can be found in a recent paper by Chatzidakis et al. (2022).

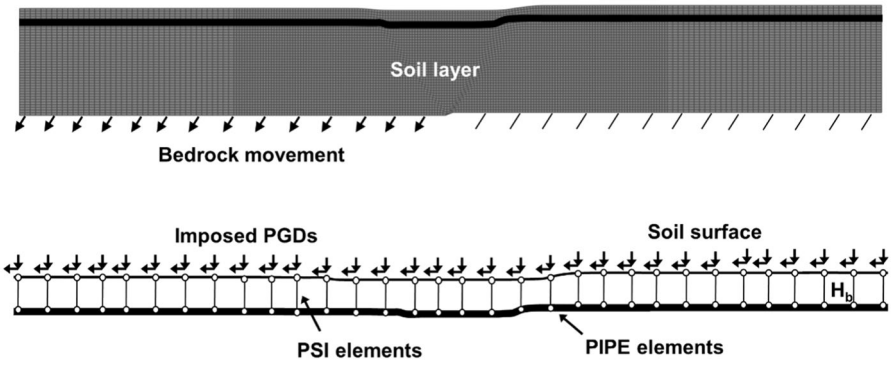

Fig. 4 Numerical model of soil – pipe interaction due to fault rupture propagation

3.2 Numerical modeling of fault-induced seismic demand on the pipe

In the present study a straight pipeline has been examined, as shown in Fig. 4. The pipeline structural performance due to tectonic faulting has been numerically investigated employing the conventional Static-Standard module of the ABAQUS software (Simulia 2014). The pipeline has been simulated using PIPE21 elements, which are two-node and in plane Timoshenko elements, allowing transverse shear deformation. For the numerical modeling of pipe-soil interaction, PSI24 elements have been selected for the axial and vertical directions, consisting of four nodes, two for the soil surface representation and two that are attached to the pipe.

PSI elements are more preferable than the conventional soil springs, since they automatically assess the soil resistance under the provisions of ALA guidelines (ALA 2001), as long as the burial depth of the pipeline and the parameters of the surrounding soil (such as friction angle, soil unit weight, etc.) are known. Moreover, PSI elements usually lead to more realistic and accurate results, as they have the capability to adjust the direction of pipe-soil interaction, and they account for large pipe movement and rotation, considering also the associated fluctuations that may be developed due to the variations of pipe embedment depth. Finally, it is important to be mentioned that the examined problem often leads to large deformation levels, and subsequently the elastic behavior of materials is exceeded. Hence, material and geometrical non-linearities have been successfully incorporated into the analyses.

Figure 4 provides a further insight on the numerical modeling of the pipeline and pipe-soil interaction. In order to achieve the optimal numerical modeling and ensure solution convergence, the pipe FE (and subsequently the PSI FE) are assigned to the same size of the soil FE model. Furthermore, a pipeline of typically infinite length is simulated to ensure the minimization of undesired boundary conditions on the edges of the FE model. The end of the pipeline, as well as the far-field PSI nodes towards the footwall soil block are fixed, whereas the opposite end and the associated far-field PSI nodes (i.e., towards the hanging wall) follow the fault movement. The PGDs in axial and vertical directions, which have been derived from the soil FE model, are imposed on the pipeline through the PSI elements, within the critical length (i.e., 4 or 8 H).

3.2.1 Experimental validation

The accuracy of the proposed pipeline FE model has been verified against the experimental investigation of Tsatsis et al. (2019) for dip-slip faulting. In particular, the experiments were based on dense Longstone sand with relative density, Dr = 90%, and dry unit weight, $\gamma = 15.68\ kN/m^3$. A scaled pipe consisting of stainless-steel grade AISI Type 444 was taken into account, with outer diameter, D = 35 mm, and thickness, t = 0.5 mm, respectively. In addition, the embedment depth of the pipe was set equal to $H_b = 0.55$ m, measured from its centerline.

Four different normalized vertical bedrock movements (i.e., h / D = 0.5, 1, 1.5 and 2, where h is the bedrock dislocation and D is the diameter of the pipe) have been investigated to compare the numerical and the associated experimental results. The axial strain in the bottom line of the pipe has been computed for each h / D ratio. Thus, Chatzidakis et al. (2022) demonstrated that although the proposed FE model slightly overestimates the tensile strains, the more critical compressive strains are accurately evaluated for the case of normal faulting. As far as reverse faults are concerned, the proposed numerical model results in overestimated tensile, as well as compressive strains. Hence, it is concluded that the proposed pipe FE model can fulfill the purposes of the current study.

4 Numerical results and discussion

A typical and realistic gas pipeline has been taken into account, where D = 0.9144 m (36 in), and t = 19.05 mm (0.75 in), respectively, i.e., D/t = 48. The pipeline has been assumed to be buried 2 m below the ground surface, as measured from the pipe centerline (H_b = 2 m). The total length of the pipeline (i.e., a few kilometers), has been defined according to the length of the examined soil deposit, in order to minimize the impact of imposed boundary conditions. Regarding the pipe steel material, the commonly-used API 5 L X65 steel grade has been selected, characterized by the Ramberg – Osgood plasticity as follows:

$$\varepsilon = \frac{\sigma}{E} + \frac{\alpha_r \sigma_0}{E}\left(\frac{\sigma}{\sigma_0}\right) \tag{6}$$

where Young's Modulus, E = 210 GPa; Poissons' ratio, v = 0.3; yield stress, $\sigma_0 = 490$ MPa; hardening exponent, n = 20 and yield offset, $\alpha_r = 1.0$.

As mentioned earlier, pipe-soil interaction was simulated with PSI FE elements. These elements are based on the analytical equations of ALA guidelines, in terms of the peak friction angle, φ_p, the coefficient of lateral earth pressure at rest, $K_0 = 1 - \sin\varphi$, as well as the type of external pipe coating, f, which has been set equal to 0.7, corresponding to smooth steel. Soil cohesion has been set equal to 0. Finally, drained conditions have been assumed, since the presence of water could add further complexity to the problem under investigation (Ng et al. 2012; Ahmadi et al. 2018a, b). Nevertheless, it is important to note that the value of peak friction angle has been conservatively utilized herein for the calculation of pipe distress. In reality, the surrounding soil yields and consequently friction angle is reduced in cases of large bedrock dislocation, as it has been shown in the soil constitutive model.

An extensive parametric investigation has been carried out to evaluate the pipe kinematic distress. Particularly, a number of FE analyses have been undertaken for both normal and reverse faulting, and dip angles $\alpha = 30^o$ and 60^o, as well. A uniform sandy

stratum of thickness, H, ranging from 20 to 100 m, has been subjected to different levels of bedrock dislocation, corresponding to earthquake magnitudes M = 6.5, 7.0 and 7.5 (according to the empirical correlation proposed by Wells and Coppersmith (1994)).

The overlying soil stratum is composed of three idealized sand types, namely Loose Sand (LS), Medium Sand (MS) and Dense Sand (DS). Table 1 presents the mechanical properties of the three sand materials. It is noted that LS does not experience strain softening and consequently the critical states of friction and dilation angles have been utilized, as proposed by Loukidis et al. (2009). Moreover, soil non-linear behavior has been realistically captured applying the adopted constitutive model, whereas soil strength has been assumed to linearly increase with respect to soil depth z, as proposed from Chatzidakis et al. (2022).

In the following plots, soil strain contours are also included to represent fault rupture propagation within the soil layer and resulting plastic deformations, while more details regarding the geotechnical aspects of fault rupture propagation through the soil layer are given in Makrakis et al. (2023). Herein, the emphasis is given on pipe distress and the results are presented in terms of: (i) the ratio x / H, which indicates the location along the soil FE model, x, normalized in terms of soil layer thickness, H, and (ii) the pipe deformations. The latter have been computed in terms of tensile and compressive strains (i.e., ε_{max} and ε_{min}, respectively), which are determined as the combination of pipe axial and bending loadings due to fault motion. It is noted that in the subsequent plots (i.e., Figs. 5, 6, 7, 8, 9, 10, 11 and 12) the center of the model is considered as the origin of the x axis.

In order to be comparable with existing limit state criteria, which are provided by the international standards and norms, (e.g., EC8 - Part 4 (CEN 2006) and ALA (ALA 2001)) pipe tensile strains are related to maximum positive strains, while compressive strains are presented in terms of minimum negative strains. It is worth noting that the results presented in the sequence refer to pipe deformations observed at the top or bottom of the pipe cross-section. Moreover, the majority of the following graphs refer to a reference case model (i.e., M = 7.0, H = 20 m, $\alpha = 30^o$ and Medium Sand). Finally, a very useful comparison has been carried out between the case where the pipeline is (rather unrealistically) laid directly on bedrock (i.e., "Bedrock") and when it is buried inside the overlying soil stratum. It is noted that fragility analysis could be performed taking into account various uncertainties involved in structural integrity assessment by performing Monte Carlo simulations that have also been applied in other types of lifelines (e.g., Nuti et al. 2010; Fragiadakis et al. 2013).

4.1 Impact of soil properties

Pipeline structural performance may be significantly affected from different soil stratum properties. Herein, the impact that the three idealized types of sand (i.e., LS, MS, and DS), whose properties are summarized in Table 1, may have on pipe kinematic distress, has been investigated. It is noted that the numerical analyses correspond to the reference case model (M = 7.0, H = 20 m, $\alpha = 30^o$), which has been subjected to dip-slip fault motion (i.e., normal and reverse). Figures 5 and 6 clearly demonstrate that the structural performance of a pipeline that is buried inside a soil stratum of H = 20 m has been affected, since outcropped shear failure zones occurred for all the examined sand types. Additionally, the pipeline subjected to normal faulting has been distressed due to both primary and secondary rupture

Table 1 Mechanical properties of the soil stratum

Sand	Soil density ρ (t/m^3)	Elastic modulus E(z) (MPa)	Poisson's ratio v (–)	Friction angle $\varphi_p - \varphi_{res}$ (°)	Dilation angle $\psi_p - \psi_{res}$ (°)
Loose	1.6	5 + 0.75 z	0.33	30	0
Medium	1.8	10 + 1.5 z	0.33	34–30	6–0
Dense	2.0	20 + 3 z	0.33	39–30	11–0

patterns, as compared to reverse faulting, where only primary outcropped fault rupture propagation paths can be observed.

Another important remark is that a buried pipeline inside a soil stratum consisting of DS, has experienced higher absolute values of both tensile and compressive strains, as compared to MS and LS, regardless of fault type. This is attributed to the stiffer and heavier DS. These results are in agreement with the findings of similar studies (e.g., Özcebe et al. (2017)). Additionally, it is evident from Figs. 5 and 6 that the presence of a MS or LS soil deposit leads to a substantial reduction of pipe strains, as compared to the case where the pipeline is directly laid on bedrock (i.e., "Bedrock"), regardless of fault type. The latter is more pronounced for the case of reverse faulting (i.e., Fig. 6a and b). In contrast, the presence of overlying soil deposit consisting of DS has led to considerably larger values of both tensile and compressive strains, in comparison to the ones that correspond to bedrock. This can be clearly observed in tensile strains due to normal faulting (i.e., Fig. 5a). Therefore, it is evident that soil deposits consisting of LS may have a beneficial impact on the structural behavior of buried pipelines, thus comprising a useful mitigation measure in real-life projects.

4.2 Impact of dip angle

Fault dip angle constitutes a critical factor that may considerably affect the structural integrity of a pipeline, in terms of kinematic distress. The reference model (i.e., H = 20 m, M = 7.0 and Medium Sand) has been subjected to dip-slip faulting for two different dip angles (i.e., $\alpha = 30°$ and 60°). Figures 7 and 8 indicate that the gravity graben, which has been formed for normal faulting and $\alpha = 30°$, due to the antithetic primary and secondary rupture patterns, has affected the structural behavior of the pipeline. Particularly, a different deformation profile has been revealed, as compared to normal faulting and $\alpha = 60°$, as well as to the two examined dip angles of reverse faulting. Moreover, Figs. 7a and 8a demonstrate that the pipeline has experienced considerably higher values of tensile strains for the case of normal faulting, as compared to reverse fault motion, regardless of dip angle value. This is due to the fact that normal faulting is dominated by bending and tension, thus leading to pipeline elongation.

Accordingly, as shown in Figs. 7b and 8b, the examined pipeline has been excessively distressed in compression due to reverse faulting, as compared to normal faulting. The latter is attributed to the mechanism of reverse dislocation and is completely consistent to other studies, e.g. Joshi et al. (2011). Furthermore, it is noted that the presence of overlying soil deposit seems to play a key role only in reverse faulting and especially for $\alpha = 60°$, since pipe strains near the failure zone have been considerably reduced, as compared to bedrock. Finally, it is important to be mentioned that the high inclination that characterizes

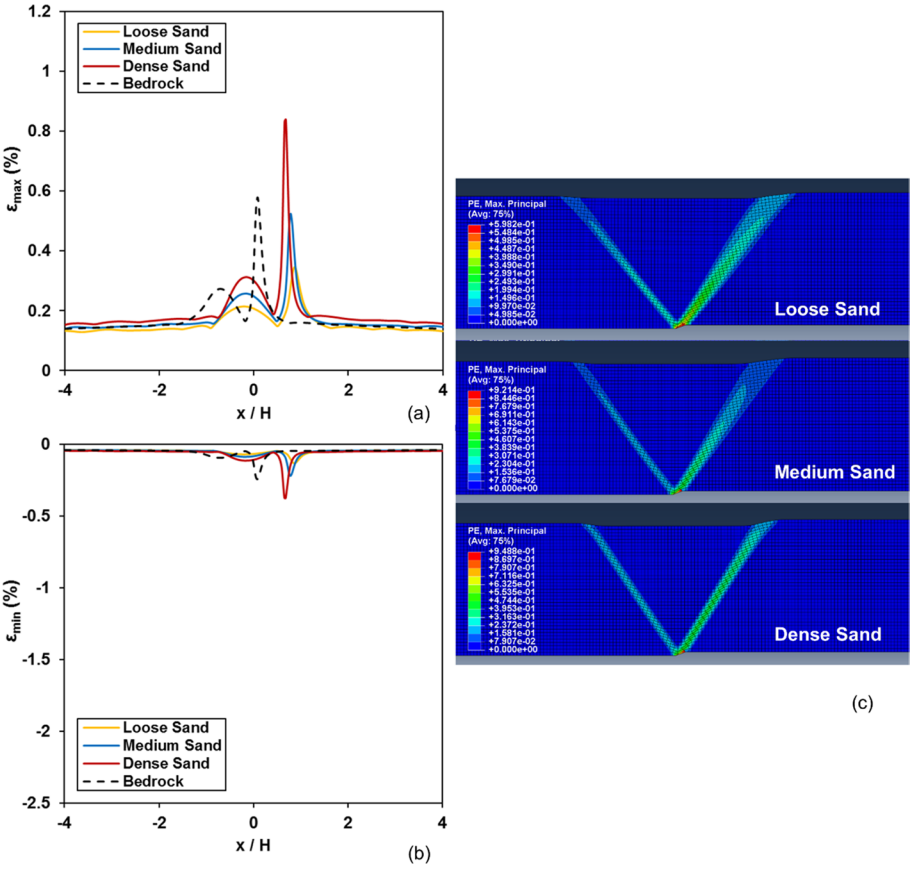

Fig. 5 Impact of soil properties for normal fault: tensile (**a**) and compressive (**b**) pipe strains and plastic deformations (**c**)

the rupture failure for reverse faulting and $\alpha = 30°$ (i.e., Fig. 8a and b) has shifted notably to the left on the horizontal axis the corresponding deformation profile of the pipeline.

4.3 Impact of soil layer thickness

The rocky part of Earth's crust is usually covered from thick to very thick soil strata, depending on local site conditions. The current study has investigated the structural behavior of the pipeline considering that the bedrock is realistically covered by an overlying soil layer of height, H, that ranges from 20 to 100 m. Judging from similar analyses in the literature, soil layers of that thickness have concentrated great research interest (Bray et al. 1994; Taniyama and Watanabe 2002; Loukidis et al. 2009), since soil covers of thickness greater than 100 m are expected to have a minor impact on a pipeline crossing at the ground surface. The reference model (i.e., M = 7.0, $\alpha = 30°$ and Medium Sand) has been subjected to dip - slip faulting.

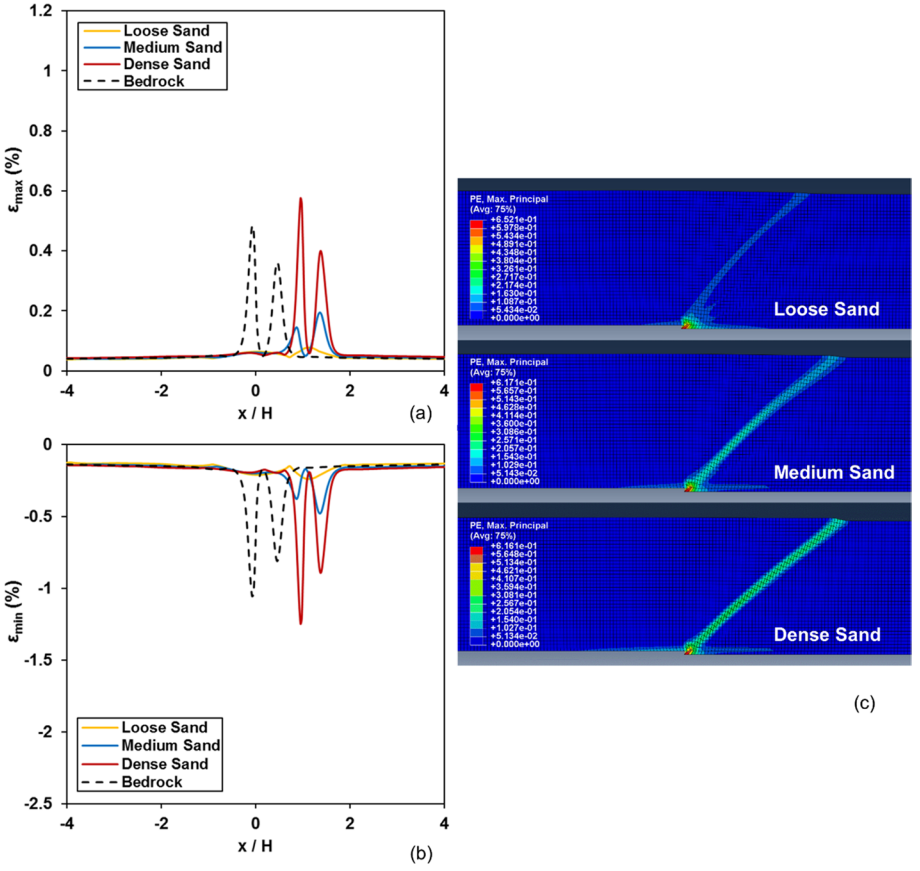

Fig. 6 Impact of soil properties for reverse fault: tensile (**a**) and compressive (**b**) pipe strains and plastic deformations (**c**)

Figure 9 displays that the pipeline has been affected by both (primary and secondary) rupture propagation paths that have been outcropped, regardless of soil layer thickness. It can be clearly observed that the presence of soil cover, regardless of its thickness, has not acted beneficially the development of pipe strains, since marginal differences occurred between the three examined soil layer thicknesses and the bedrock as well. The latter can be explained considering the local soil irregularities located at ground surface that might have led to slightly larger strains for H = 50 m and H = 100 m, respectively.

Oppositely to normal fault motion, Fig. 10 illustrates that the 20 m - thick soil stratum that is subjected to reverse dislocation has notably absorbed pipe strains, whereas for H = 50 m and 100 m, respectively, where fault outcropping has not occurred, pipeline experienced very low strains, as it was expected.

4.4 Impact of earthquake magnitude

It is evident that the level of fault offset constitutes a critical factor for the integrity of large - scale facilities, such as pipelines. As it has already been mentioned, the level of

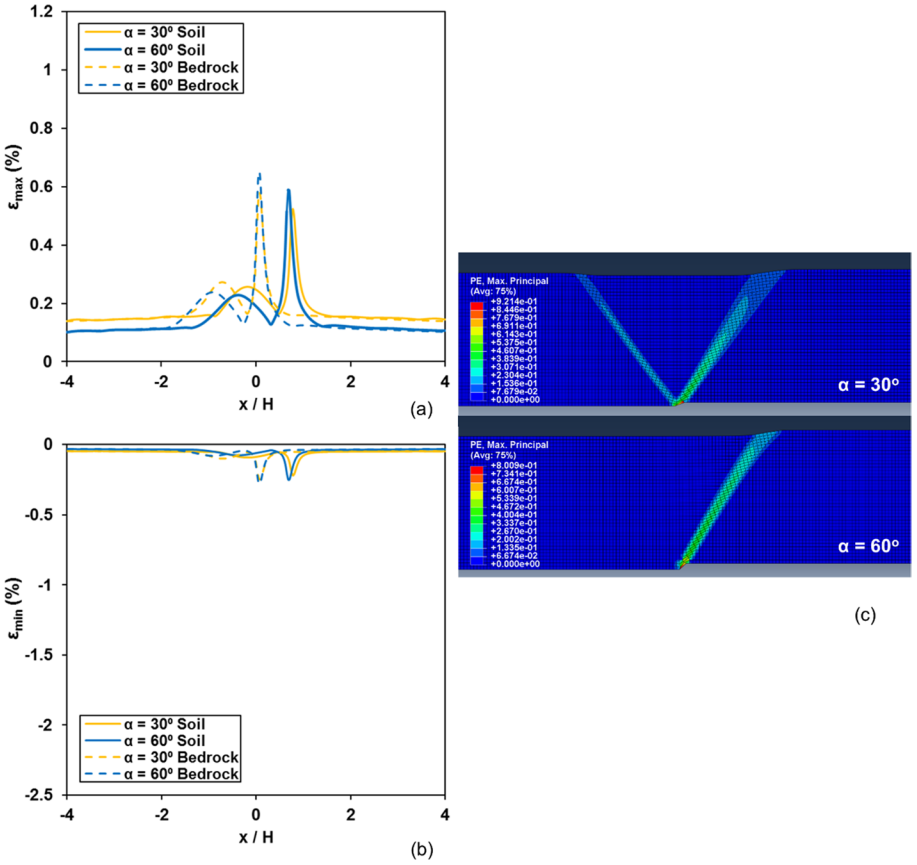

Fig. 7 Impact of dip angle for normal fault: tensile (**a**) and compressive (**b**) pipe strains and plastic deformations (**c**)

bedrock dislocation has been directly correlated with earthquake magnitude. Consequently, the reference case model (i.e., H = 20 m, α = 30°, Medium Sand) has been utilized to investigate the pipe structural performance in terms of strains, in terms of three different earthquake magnitudes (i.e., M = 6.5, 7.0 and 7.5).

As can be seen from Figs. 11 and 12, higher values of earthquake magnitude have led to excessive pipe deformation, regardless of fault type. Particularly, according to Fig. 11, normal faulting that corresponds to M = 7.5 has resulted in significantly larger pipe tensile strains, as compared to M = 7.0 and M = 6.5. The latter is not so pronounced for compressive strains. Additionally, note the significant impact of the secondary rupture failure for M = 7.5, that has resulted in excessive pipe strains along the whole fault plane. However, in the vicinity of the shear rupture zone, it should be stressed that the presence of overlying soil cover has detrimentally affected the structural performance of the pipeline in tension.

Regarding reverse fault motion, it should be stressed that the specific steel grade material could not withstand the excessive pipe deformations corresponding to M = 7.5. Thus, Fig. 12 presents pipe strains only for M = 6.5 and 7.0. It is evident that very low pipe strains have been developed for M = 6.5, due to the not-outcropped rupture failure. Nonetheless,

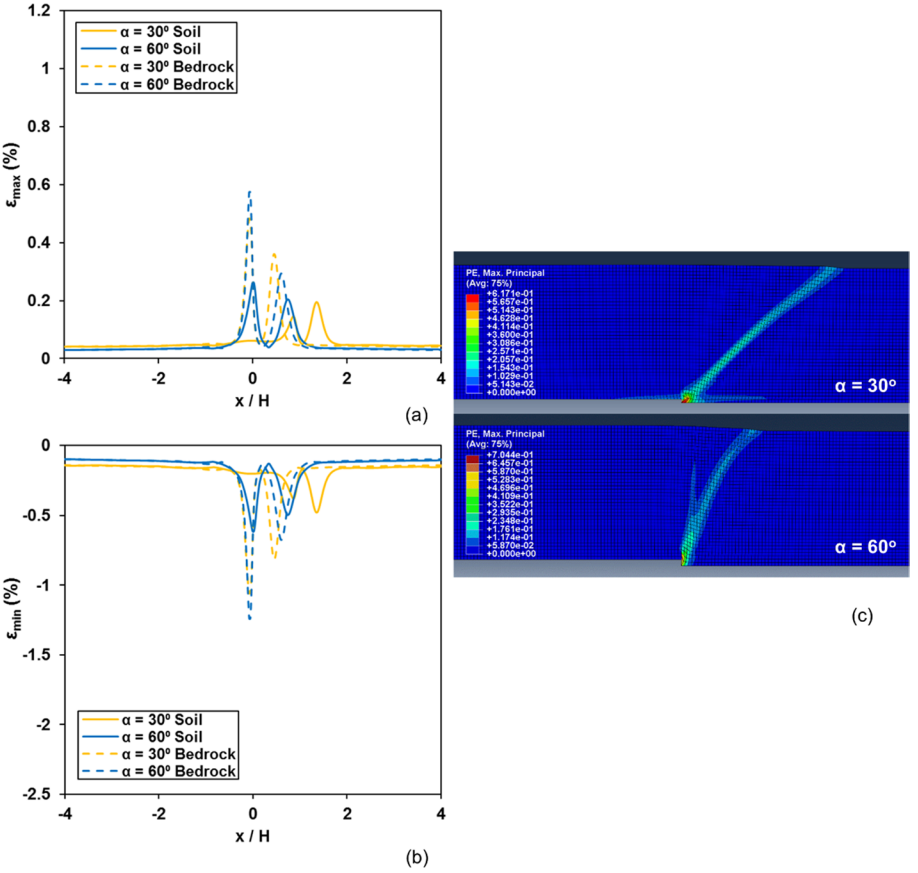

Fig. 8 Impact of dip angle for reverse fault: tensile (**a**) and compressive (**b**) pipe strains and plastic deformations (**c**)

it is noteworthy that the presence of a 20 m - thick soil cover has remarkably absorbed both pipe tensile and compressive strains, for M = 7.0.

5 Correlation between earthquake magnitude and pipe strains

In the conducted numerical analyses different earthquake magnitudes (i.e., in terms of bedrock dislocation), fault types, fault dip angles, as well as the presence (or not) of overlying soil cover of varying thickness and soil mechanical properties have been considered. Subsequently, the pipeline's structural behavior, in terms of maximum absolute pipe strains (i.e., tensile and compressive), has been correlated with earthquake magnitude. It is recalled that of the main aims of this study is to create useful charts and tables for the preliminary seismic design of pipelines, capable of directly predicting pipe deformations for different earthquake magnitudes, taking into account all these critical factors.

The existing limit states provided by international standards and regulations (e.g., ALA (2001) and EC8 - Part 4 (CEN 2006), have been utilized for comparison reasons. On the one

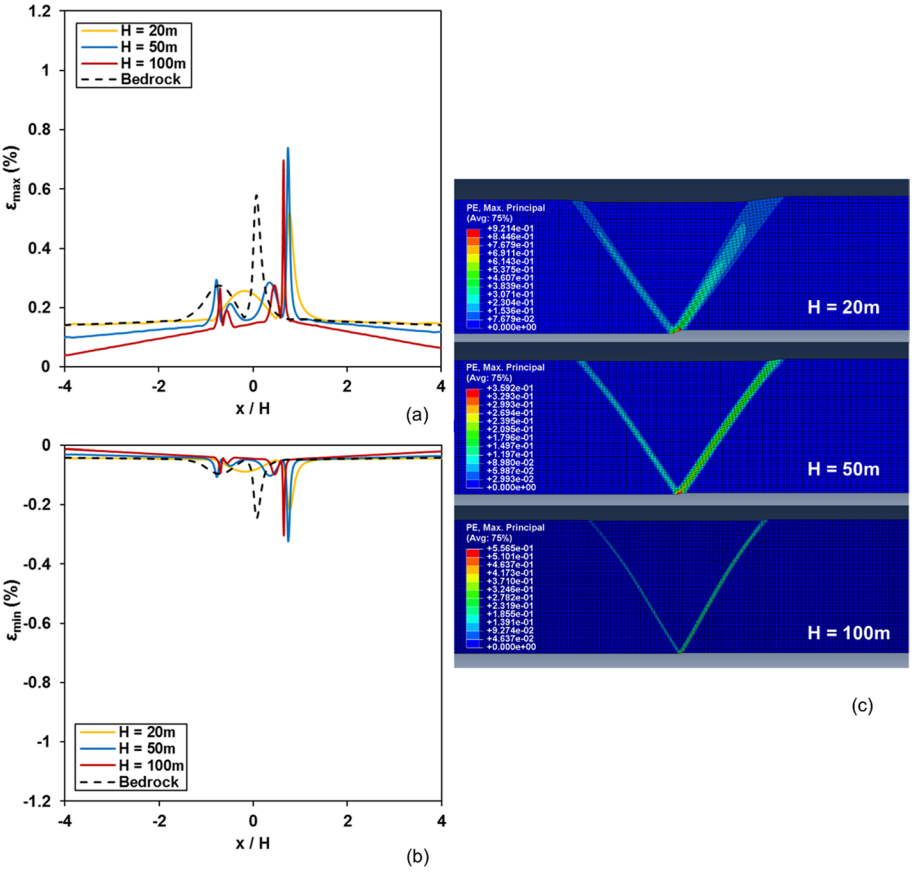

Fig. 9 Impact of soil layer thickness for normal fault: tensile (**a**) and compressive (**b**) pipe strains and plastic deformations (**c**)

hand, ALA guidelines have defined two categories to describe pipe strains, namely "operable" and "pressure integrity". As far as operable category is concerned, the critical pipe tensile strain has been set equal to 2%, whereas the compressive strain limit is denoted by Eq. (7). Regarding the pressure integrity category, 4% has been established as the allowable pipe tensile strain, while strain in pipe compression is computed from Eq. (8). On the other hand, the provisions of EC8 have set the longitudinal pipe tensile strain limit equal to 3%, whereas Eq. (9) denotes the allowable pipe compressive strain:

$$0.50\left(\frac{t}{D'}\right) - 0.0025 + 3000\left(\frac{pD}{2Et}\right)^2 \tag{7}$$

$$1.76\left(\frac{t}{D}\right) \tag{8}$$

$$\min\{1\%, 20t/r(\%)\} \tag{9}$$

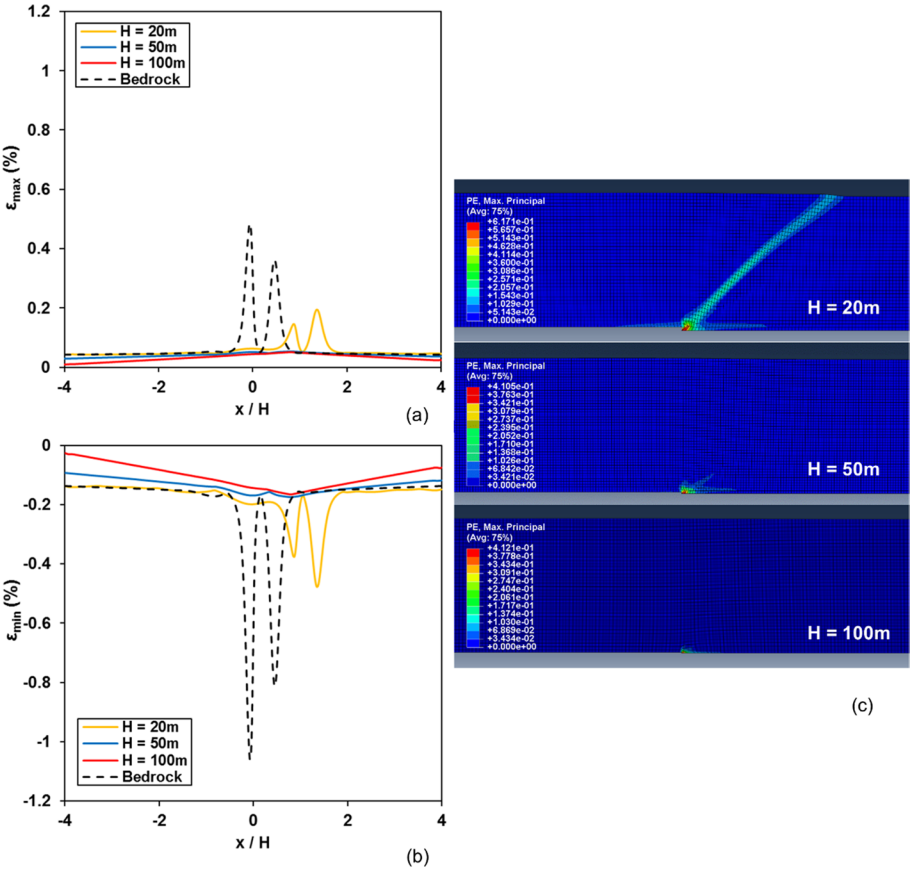

Fig. 10 Impact of soil layer thickness for reverse fault: tensile (**a**) and compressive (**b**) pipe strains and plastic deformations (**c**)

where D and t denote the pipe external diameter and thickness, respectively, and p represents the pipe internal pressure.

It is worth noticing that the worst-case scenario of a pipeline that is not in operation (pipe internal pressure equal to 0 kPa) has been examined herein. In addition, D´ is calculated from Eq. (10) and accounts for cross-section ovalization effects (ALA 2001):

$$D' = \frac{D}{1 - \frac{3}{D}\left(D - D_{\min}\right)} \tag{10}$$

However, since the undertaken analyses have been conducted utilizing two-dimensional finite elements, cross-section ovalization effects have not been taken into account. For this reason, the current study adopted the more conservative "operable" strain limits, since large strain limits may lead to the occurrence of critical modes of failure, such as local buckling, which cannot be accurately predicted via 2D numerical analyses.

Figures 13, 14, 15 and 16 depict the maximum absolute pipe strains, the allowable pipe strain limits from the relative standards and guidelines, and they are both plotted in terms

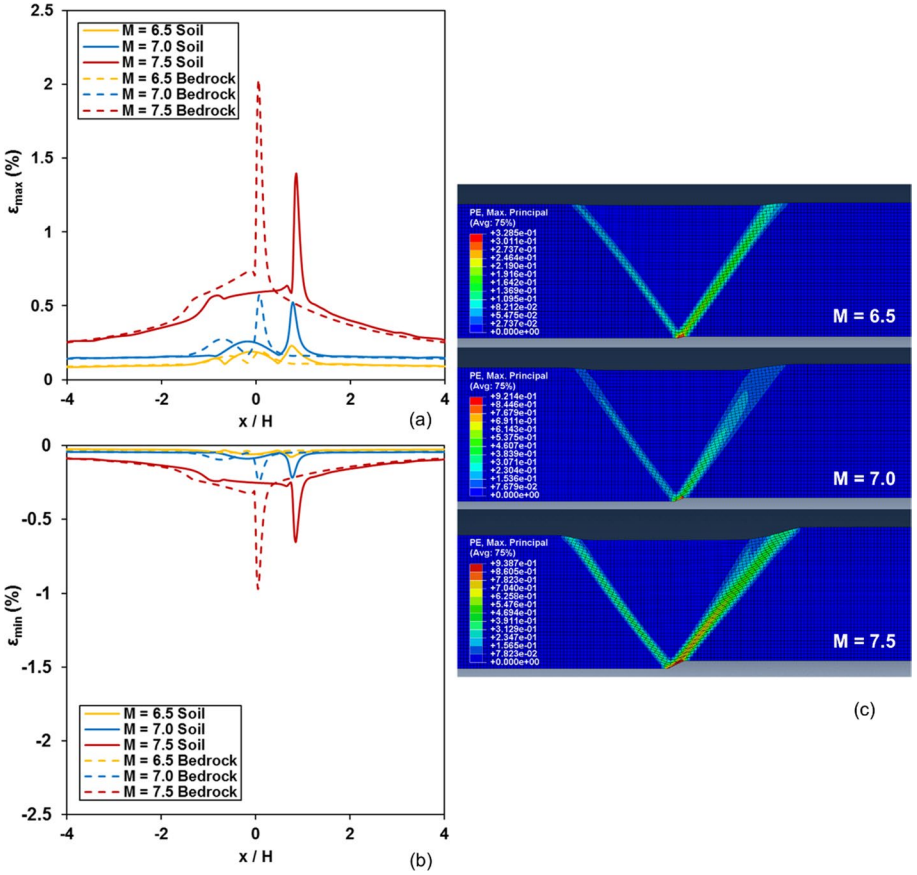

Fig. 11 Impact of earthquake magnitude for normal fault: tensile (**a**) and compressive (**b**) pipe strains and plastic deformations (**c**)

of earthquake magnitude. As far as normal faulting is concerned, Figs. 13 and 14 clearly reveal a mild linear increase from M = 6.5 to M = 7.0 and a sharper one from M = 7.0 to M = 7.5, for both tensile and compressive pipe strains, regardless of sand type, dip angle and soil cover thickness. Nonetheless, as earlier stated, the selected steel grade could not withstand the excessive pipe deformations corresponding to M = 7.5 and consequently, Figs. 15 and 16 demonstrate pipe strains only for M = 6.5 and 7.0.

According to Figs. 13, 14, 15 and 16 and a soil layer consisting of DS or MS has generally resulted in larger absolute maximum strains, compared to LS, for both the examined fault types and dip angles, regardless of soil layer thickness. Indicatively, a pipeline which is buried inside a LS soil deposit of thickness H = 20 m and subjected to normal faulting with dip angle equal to 60° and bedrock dislocation corresponding to M = 7.0, experienced almost 65% and 60% lower absolute maximum tensile and compressive strains, respectively, than the corresponding ones for the case of a DS soil deposit. Accordingly, a pipeline subjected to reverse fault offset of the same characteristics as before (i.e., LS, H = 20 m, α = 60° and M = 7.0) exhibited 70% and 65% lower tensile and compressive strains, respectively, as compared to DS.

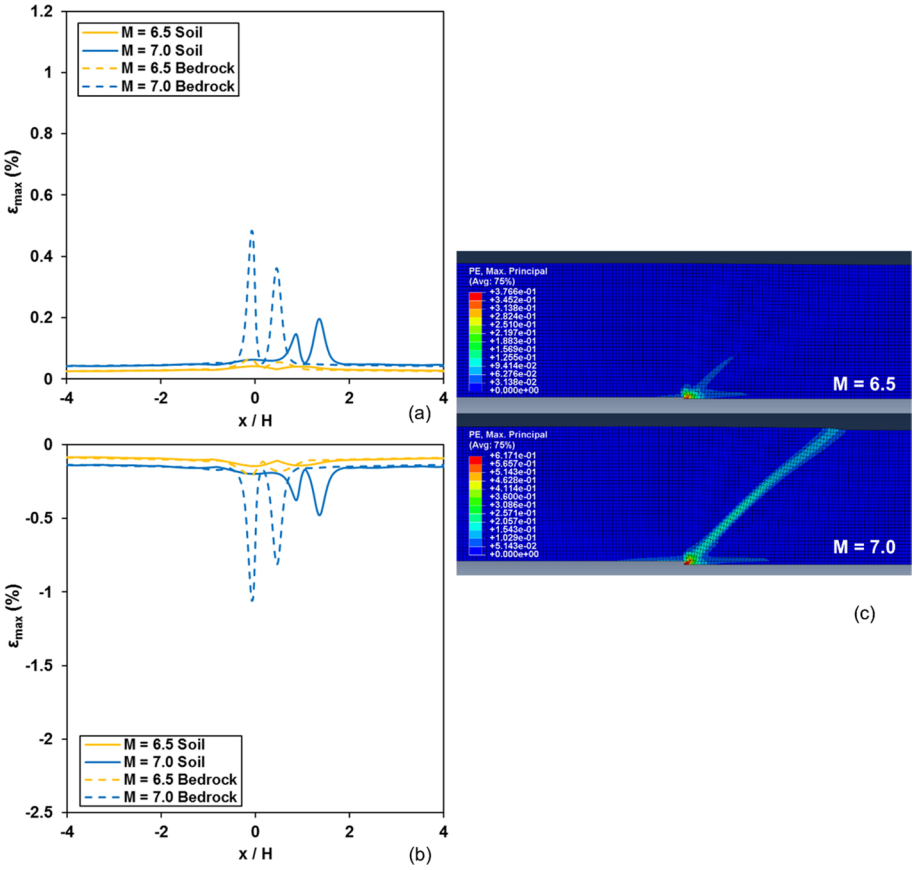

Fig. 12 Impact of earthquake magnitude for reverse fault: tensile (**a**) and compressive (**b**) pipe strains and plastic deformations (**c**)

Results shown in Fig. 13 indicate that the presence of overlying soil bed has prevented non - allowable pipe tensile strains for LS and MS, regardless of earthquake magnitude, dip angle and soil layer thickness, since the critical limits established both from ALA and EC8 respectively, have not been exceeded. Contrariwise, for the case where the examined pipeline is buried inside a DS soil cover and subjected to normal fault motion of dislocation corresponding to M = 7.5, non - allowable tensile strains (up to 0.75% larger - almost 40% percentage change - than the ALA limits) have been developed for all the examined soil layer thicknesses and dip angles. Nonetheless, it is worth noticing that only a 100 m thick DS soil deposit, which is subjected to normal fault motion dipping at $\alpha = 60°$, has resulted in slightly lower pipe tensile strains than the critical limit of ALA guidelines (i.e., 0.1% lower – 4% percentage change). As far as reverse fault motion is concerned, Fig. 15 demonstrates that pipe tensile strains are at least 1.4% lower than the established limits (70% percentage change) for all the examined sand types, dip angles, soil layer thicknesses and earthquake magnitudes. The latter is expected, and it is attributed to the reverse faulting mechanism, which tends to distress the pipeline in compression.

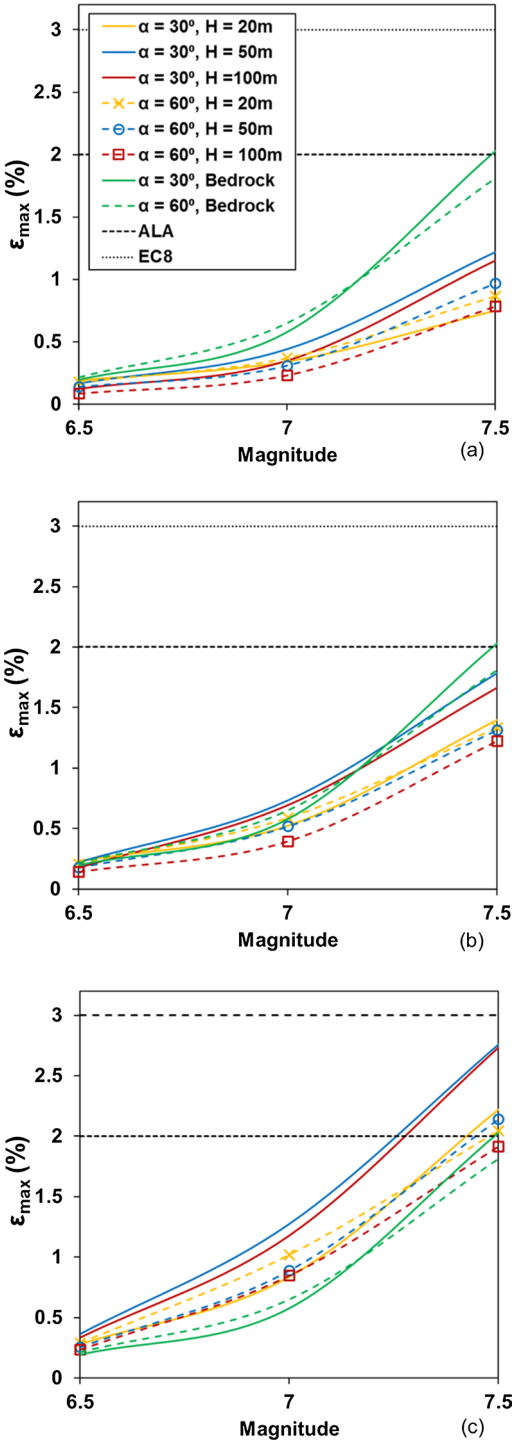

Fig. 13 Correlation of pipe tensile strains and earthquake magnitude for normal fault propagating through: **a** loose sand, **b** medium sand, and **c** dense sand

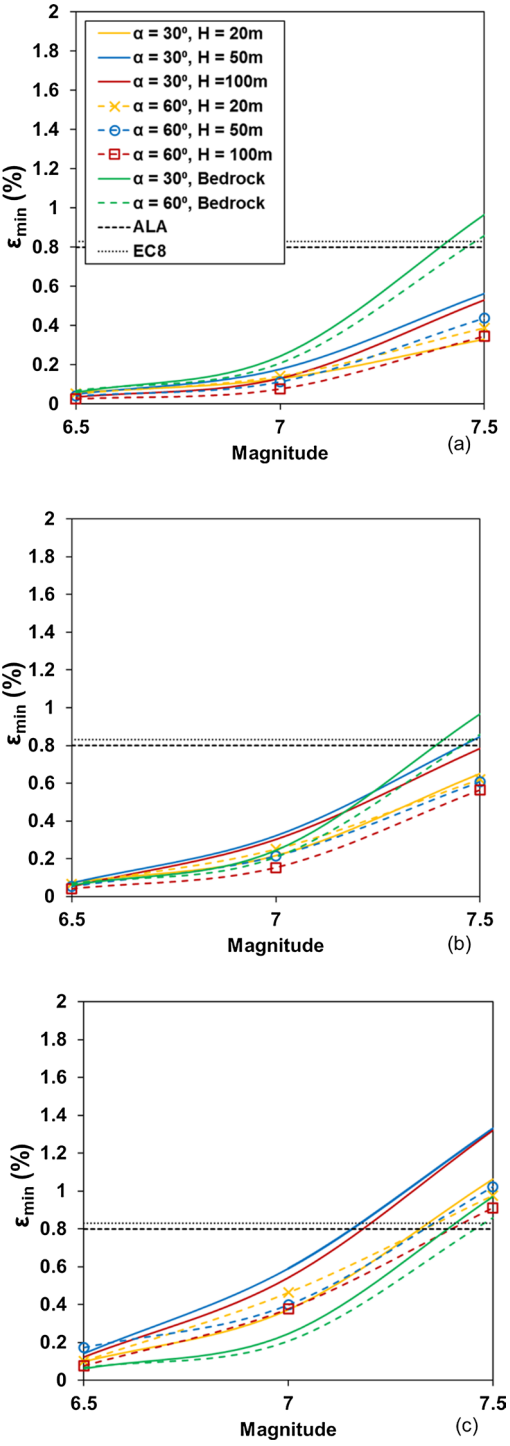

Fig. 14 Correlation of pipe compressive strains and earthquake magnitude for normal fault propagating through: **a** loose sand, **b** medium sand and **c** dense sand

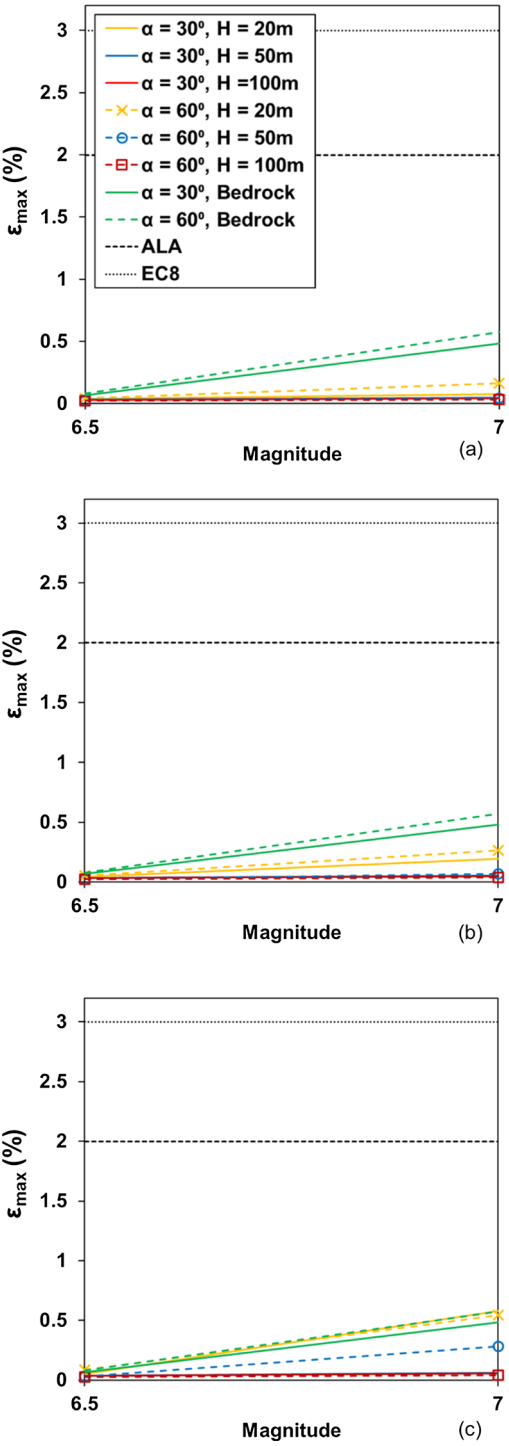

Fig. 15 Correlation of pipe tensile strains and earthquake magnitude for reverse fault propagating through: **a** loose sand, **b** medium sand and **c** dense sand

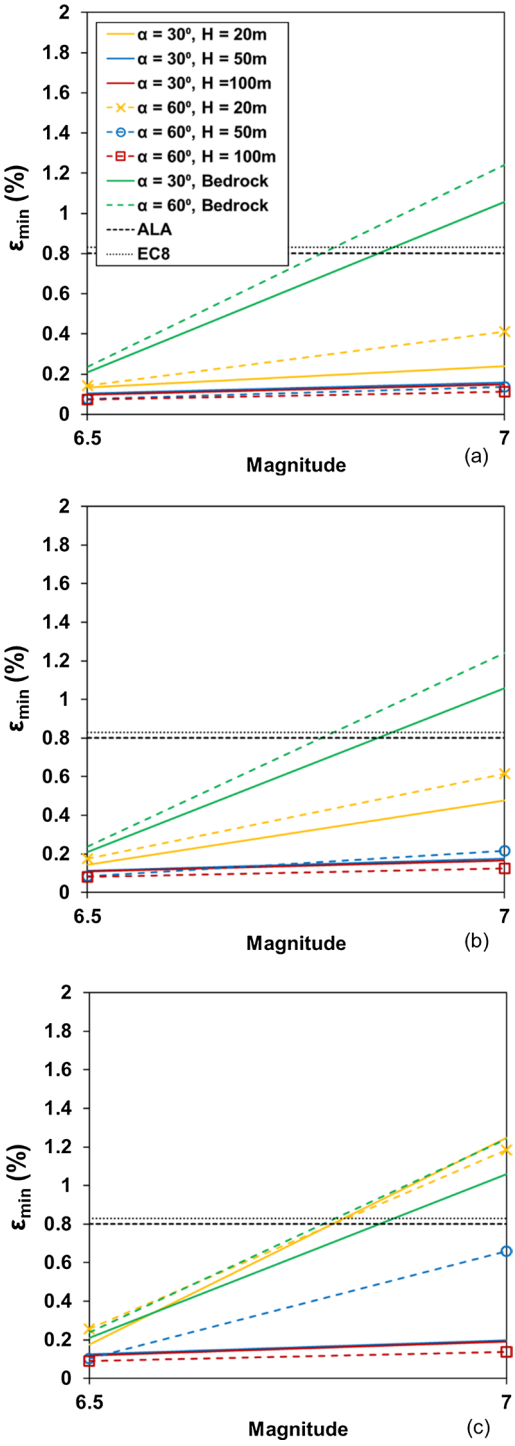

Fig. 16 Correlation of pipe compressive strains and earthquake magnitude for reverse fault propagating through: **a** loose sand, **b** medium sand and **c** dense sand

Additionally, with respect to pipe compressive strains due to normal faulting, it can be observed from Fig. 14 that the presence of LS overlying soil deposit has played a beneficial role. Particularly, non-allowable pipe deformation was completely absorbed for M = 7.5, regardless of soil layer thickness and dip angle, since at least 0.24% lower compressive strains than the slightly more conservative ALA limits (30% percentage change) have been reported. Conversely, DS soil layer subjected to normal fault motion has not prevented non-allowable pipe deformation, as for M = 7.5, all the examined scenarios have resulted in larger compressive strains than the ALA and EC8 limits. It is noteworthy that for M = 7.5 and α = 30°, a pipeline buried inside a 50 and 100 m thick soil deposit experienced 65% larger compressive strains than the ALA limits. Moreover, according to Fig. 16, the presence of LS, as well as MS, soil cover has prevented non-allowable pipe compressive strains for the case of reverse faulting, since at least 0.2% lower tensile stains than ALA limits (23% percentage change) have been observed.

Figures 13 and 14 illustrate that normal fault motion with dip angle α = 30° has generally resulted in greater levels of absolute maximum pipe strains, as compared to α = 60°, regardless of sand type and earthquake magnitude. However, the latter is more pronounced for thick soil deposits (i.e., H = 50 and 100 m), where for H = 50 m, the dip angle α = 30° has resulted in 26% larger tensile and compressive strains, as compared to α = 60°. Regarding H = 100 m, the α = 30° has led to 32% larger tensile and compressive strains, as compared to α = 60°. On the other hand, Figs. 15 and 16 demonstrate that MS and LS soil deposits of H = 20 m that are subjected to 60°-reverse-dislocation have generally produced larger tensile and compressive strains, than α = 30°.

Moreover, in the case of normal faulting, increasing 2.5- or 5-times the overlying soil layer thickness (i.e., from 20 to 50 m and from 20 to 100 m) has played a beneficial role only for relatively low values of earthquake magnitude (i.e., M = 6.5) and soil covers consisting of LS and MS, regardless of dip angle. Indicatively, pipe deformation has been absorbed up to 50% for 5-times increase and up to 22% for 2.5-times increase of soil layer thickness. However, for greater earthquake magnitudes (i.e., M = 7.0 and M = 7.5) and α = 60°, only the 5-times increase of soil layer thickness has absorbed pipe strains, regardless of sand type, leading for instance to 17% and 6.5% lower tensile and compressive strains, respectively, for the case of DS. Due the complicated rupture patterns that have been developed for dip angle equal to 30°, the increase of soil layer thickness has even led to the increase of the absolute maximum pipe strains. Conversely, a considerable impact of soil layer thickness has been reported for reverse faulting, since both a 2.5-times and a 5-times thicker soil deposit, as well, reduced pipe strains up to 80% regardless of earthquake magnitude, sand type and dip angle.

Finally, the current study investigated the case where the pipeline is laid directly on bedrock and subjected to fault motion (without the presence of overlying soil deposit), as compared to the case where rock outcrop is covered from soil stratum. This comparison is of utmost importance from a practical engineering viewpoint. Thus, results from Fig. 14 demonstrate that for the case where the pipeline is placed at bedrock and subjected to normal fault motion corresponding to M = 7.5, non-allowable compressive strains equal to 0.97% (0.14% larger – almost 17% percentage change – than ALA limit) and 0.86% (0.03% larger – almost 3.5% percentage change) were developed for α = 30° and 60°, respectively. However, the presence of a LS soil cover of H = 20 m has reduced the corresponding strains by 66% and 55% (reduced strains equal to 0.33% and 0.39%), respectively.

As far as reverse fault motion is concerned, Figs. 15 and 16 reveal a detrimental impact of a LS soil deposit of thickness equal to 20 m. In particular, pipe tensile strains for M = 7.0 have been reduced by 85% and 72%, for α = 30° and 60°, respectively, as compared to the

case where the pipeline is laid directly on bedrock. Additionally, a similar decrease of pipe compressive strains can be clearly seen for M = 7.0 (i.e., 78% and 67%, for α = 30° and 60° respectively). Nonetheless, it is worth noticing that the presence of thicker soil layers consisting of LS (i.e., H = 50 and 100 m) has reduced pipe tensile and compressive strains up to 95%, for both the examined dip angles.

In order to illustrate in a more comprehensive and easily applicable in practice manner the correlation of the tensile and compressive pipe strains with earthquake magnitude, various statistical distributions have been tested, aiming to select the one that accurately approximates the datasets presented in Figs. 13, 14, 15 and 16. This process has been performed taking into account the value of R-squared statistical coefficient, which constitutes a standard measure of fitting accuracy. The second-order polynomial expression presented in Eq. (11), has been selected as the most suitable statistical distribution, since the corresponding R^2 was very close to unity, indicating that the regression predictions perfectly fit the obtained datasets:

$$\varepsilon(\%) = \alpha \cdot M^2 + \beta \cdot M + \gamma \tag{11}$$

where α, β and γ are defined as curve fitting coefficients, ε (%) denotes the pipe strain expressed as percentage, while M is the earthquake moment magnitude.

Tables 2 and 3 present the fitting parameters of the proposed empirical relationships for dip-slip faulting, dip angles 30° and 60°, three levels of fault offset corresponding to M = 6.5, 7 and 7.5 (for normal fault only), and soil layer thickness ranging from 20 to 100 m. Note that the case of rock outcrop (without presence of overlying soil stratum) is also included with soil layer thickness equal to 0.

Table 2 Curve fitting parameters for compressive and tensile (in parentheses) strains for normal fault

Dip angle (°)	Soil layer thickness (m)	$\varepsilon(\%) = \alpha \cdot M^2 + \beta \cdot M + \gamma$ (M = 6.5, 7.0 and 7.5)								
		Loose sand			Medium sand			Dense sand		
		α	β	γ	α	β	γ	α	β	γ
30	0	1.1 (2.1)	–14.1 (–28.1)	46.6 (92.5)	1.1 (2.1)	–14.1 (–28.1)	46.6 (92.5)	1.1 (2.1)	–14.1 (–28.1)	46.6 (92.5)
	20	0.3 (0.5)	–3.4 (–6.6)	11.0 (21.5)	0.6 (1.2)	–7.6 (–15.1)	24.9 (49.5)	0.8 (1.6)	–10.6 (–21.1)	34.2 (68.0)
	50	0.5 (1.0)	–6.7 (–13.0)	21.8 (42.3)	0.5 (1.1)	–6.9 (–13.6)	21.8 (42.8)	0.6 (1.1)	–6.9 (–13.6)	20.5 (40.7)
	100	0.6 (1.2)	–8.0 (–15.2)	26.3 (49.8)	0.5 (0.9)	–5.8 (–11.2)	18.0 (34.6)	0.7 (1.4)	–8.8 (–17.5)	27.3 (54.1)
60	0	1.0 (1.5)	–13.5 (–18.7)	44.7 (60.7)	1.0 (1.5)	–13.5 (–18.7)	44.7 (60.7)	1.0 (1.5)	–13.5 (–18.7)	44.7 (60.7)
	20	0.3 (0.6)	–4.0 (–7.8)	13.1 (25.2)	0.4 (0.7)	–4.6 (–9.0)	14.4 (28.1)	0.3 (0.6)	–3.3 (–6.5)	9.1 (17.7)
	50	0.5 (1.0)	–6.7 (–12.9)	22.2 (42.4)	0.5 (0.9)	–6.0 (–11.6)	19.2 (37.2)	0.8 (1.2)	–10.3 (–15.4)	33.5 (48.3)
	100	0.4 (0.8)	–5.8 (–10.6)	19.3 (35.1)	0.6 (1.1)	–7.8 (–15.0)	25.7 (49.1)	0.5 (0.9)	–5.6 (–11.1)	17.2 (33.7)

Table 3 Curve fitting parameters for compressive and tensile (in parentheses) strains for reverse fault

Dip angle (°)	Soil layer thickness (m)	$\varepsilon(\%) = \alpha \cdot M^2 + \beta \cdot M + \gamma$ (M = 6.5 and 7.0)								
		Loose sand			Medium sand			Dense sand		
		α	β	γ	α	β	γ	α	β	γ
30	0	0.0 (0.0)	1.7 (0.8)	–10.8 (–5.3)	0.0 (0.0)	1.7 (0.8)	–10.8 (–5.3)	0.0 (0.0)	1.7 (0.8)	–10.8 (–5.3)
	20	0.0 (0.0)	0.2 (0.07)	–1.3 (–0.4)	0.0 (0.0)	0.7 (0.3)	–4.2 (–1.9)	0.0 (0.0)	2.1 (1.0)	–13.8 (–6.8)
	50	0.0 (0.0)	0.1 (0.03)	–0.6 (–0.18)	0.0 (0.0)	0.1 (0.04)	–0.7 (–0.21)	0.0 (0.0)	0.1 (0.05)	–0.78 (–0.264)
	100	0.0 (0.0)	0.1 (0.03)	–0.56 (–0.17)	0.0 (0.0)	0.1 (0.03)	–0.6 (–0.19)	0.0 (0.0)	0.1 (0.05)	–0.80 (–0.263)
60	0	0.0 (0.0)	2.0 (1.0)	–12.8 (–6.4)	0.0 (0.0)	2.0 (1.0)	–12.8 (–6.4)	0.0 (0.0)	2.0 (1.0)	–12.8 (–6.4)
	20	0.0 (0.0)	0.5 (0.2)	–3.4 (–1.5)	0.0 (0.0)	0.9 (0.4)	–5.5 (–2.7)	0.0 (0.0)	1.8 (0.9)	–11.8 (–5.9)
	50	0.0 (0.0)	0.1 (0.04)	–0.7 (–0.2)	0.0 (0.0)	0.3 (0.09)	–1.6 (–0.5)	0.0 (0.0)	1.1 (0.5)	–7.1 (–3.3)
	100	0.0 (0.0)	0.07 (0.02)	–0.4 (–0.1)	0.0 (0.0)	0.08 (0.03)	–0.5 (–0.14)	0.0 (0.0)	0.1 (0.03)	–0.5 (–0.16)

6 Conclusions

The present study investigates numerically the problem of fault-pipe intersection, focusing on the structural performance of a buried gas pipeline. Based on the results of an extensive parametric investigation, the objective is to correlate the kinematic distress of the pipeline, in terms of strains, with earthquake magnitude, in terms of bedrock dislocation. The produced charts and tables are of direct practical relevance for the preliminary seismic design and route optimization of buried steel pipelines.

The decoupled FE methodology has been adopted for numerical simulations, i.e., the surrounding soil and the pipeline were simulated separately. Soil non-linearity has been realistically taken into consideration utilizing the Mohr-Coulomb constitutive model with isotropic strain softening. Both FE-based models have been successfully validated against the results of experimental programs from the literature and in the sequence, a detailed parametric investigation has been carried out, accounting for different earthquake magnitudes, fault types, fault dip angles, as well as various thicknesses and mechanical properties of the soil cover.

The good agreement of the results with the corresponding ones reported in the literature provides a reliable basis for the following concluding remarks:

- A buried pipeline inside a soil deposit consisting of Loose Sand may experience up to 60 − 70% reduced pipe strains as compared to the ones induced in case of Dense Sand. Additionally, the presence of a thin-to-medium soil layer (i.e., H = 20 m) consisting of LS can reduce absolute maximum pipe strains up to 65% and 80% for normal and reverse fault, respectively, as compared to when the pipeline is directly placed at bedrock. This practically means that overlying soil cover(s) consisting of

Loose Sand may have a beneficial impact on the structural performance of buried pipelines during fault rupture. Consequently, the use of an artificial layer of Loose Sand may act as an efficient mitigation technique in seismic regions where pipelines cross active faults.

- Given a fault dip angle $\alpha = 60°$, a considerable increase of soil layer thickness could reduce pipe strains even for excessive earthquake magnitudes and soil covers of high stiffness (i.e., 6% for M = 7.5 and DS). In contrast, for $\alpha = 30°$, the increase of soil layer thickness could even lead to the increase of pipe strains. Overall, a moderate increase of soil layer thickness might have a detrimental impact for the case of reverse faulting, since thicker soil covers could considerably absorb pipe deformation, leading up to 80% reduced pipe strains, regardless of sand type, dip angle and earthquake magnitude. Thus, it can be concluded that a pipeline could safely cross a reverse bedrock dislocation, even if exposed to excessive seismic hazard (here expressed in terms of earthquake magnitude), as long as bedrock is covered by medium - to-thick soil deposit(s).
- Normal fault with dip angle $\alpha = 30°$, has generally resulted in greater pipe deformation (compared to $\alpha = 60°$), for all the examined sand types and earthquake magnitudes. This is more pronounced for thick soil deposits (i.e., H = 50 and 100 m, respectively), where almost 30% larger strains can be observed, as compared to $\alpha = 60°$. For the case of reverse faulting and dip angle 60°, larger pipe strains have been obtained for H = 20 m, as compared to $\alpha = 30°$.

On the basis of the promising findings presented in this paper, future extensions could investigate the response of layered soil strata, taking also into account the presence of water as well as soil cohesion, as this work examined only sandy deposits. In addition, the implementation of a probabilistic approach (PFDHA), instead of the adopted deterministic methodology, can provide a more realistic assessment of the fault displacement hazard.

Author contributions All authors contributed during the preparation of this work and consent to publish it. NM Conceptualization, Methodology, Software, Validation, Investigation, Writing - Original Draft, Visualization. PNP Conceptualization, Investigation, Writing - Review & Editing, Visualization. AS Conceptualization, Methodology, Investigation, Writing - Review & Editing, Visualization. YT Conceptualization, Investigation, Writing - Review & Editing, Supervision, Project administration, Visualization.

Funding Open access funding provided by HEAL-Link Greece. This research was performed without any funding or grants from any institutions or individuals.

Data availability Data can be provided upon request.

Code availability Not applicable (a commercial software has been used).

Declarations

Conflicts of interest The authors have no conflicts of interest to declare that are relevant to the content of this article.

References

Ahmadi M, Moosavi M, Jafari MK (2018a) Experimental investigation of reverse fault rupture propagation through wet granular soil. Eng Geol 239:229–240. https://doi.org/10.1016/j.enggeo.2018.03.032

Ahmadi M, Moosavi M, Jafari MK (2018b) Experimental investigation of reverse fault rupture propagation through cohesive granular soils. Geomech Energy Environ 14:61–65. https://doi.org/10.1016/j.gete.2018.04.004

ALA (2001) Guidelines for the design of buried steel pipe. American Lifelines Alliance. American Society of Civil Engineers, Reston, VA

Anastasopoulos I, Gazetas G, Bransby MF et al (2007) Fault rupture propagation through sand: finite-element analysis and validation through centrifuge experiments. J Geotech Geoenviron Eng 133:943–958

ASCE (1984) Guidelines for the seismic design of oil and gas pipeline systems. Committee on Gas and Liquid Fuel Lifelines. American Society of Civil Engineers, New York

Bray JD (1990) The effects of tectonic movements on stresses and deformations in earth embankments. University of California, Berkley, CA, USA

Bray JD, Seed RB, Seed HB (1994) Analysis of earthquake fault rupture propagation through cohesive soil. J Geotech Eng 120:543–561

CEN (2006) Eurocode 8 - design of structures for earthquake resistance. Part 4: Silos, tanks and pipelines. European standard EN 1998-4, July 2006, European Committee for Standardization, Brussels

Chatzidakis D, Tsompanakis Y, Psarropoulos PN (2022) Kinematic distress of pipelines subjected to secondary seismic fault rupture. Soil Dyn Earthq Eng 152:107065. https://doi.org/10.1016/j.soildyn.2021.107065

Chinnery MA (1969) Earthquake magnitude and source parameters. Bull Seismol Soc Am 52:1969–1982. https://doi.org/10.1785/bssa0590051969

Demirci HE, Bhattacharya S, Karamitros D, Alexander N (2018) Experimental and numerical modelling of buried pipelines crossing reverse faults. Soil Dyn Earthq Eng 114:198–214. https://doi.org/10.1016/j.soildyn.2018.06.013

Dey S, Chakraborty S, Tesfamariam S (2020) Structural performance of buried pipeline undergoing strike-slip fault rupture in 3D using a non-linear sand model. Soil Dyn Earthq Eng 135:106180. https://doi.org/10.1016/j.soildyn.2020.106180

Fadaee M, Farzaneganpour F, Anastasopoulos I (2020) Response of buried pipeline subjected to reverse faulting. Soil Dyn Earthq Eng 132:106090. https://doi.org/10.1016/j.soildyn.2020.106090

Fragiadakis M, Christodoulou SE, Vamvatsikos D (2013) Reliability assessment of urban water distribution networks under seismic loads. Water Resour Manag 27:3739–3764. https://doi.org/10.1007/s11269-013-0378-0

Gawande K, Kiran R, Cherukuri HP (2019) A numerical study of the response of buried steel pipelines undergoing strike-slip fault. Eng Fail Anal 102:203–218. https://doi.org/10.1016/j.engfailanal.2019.04.026

Ha D, Abdoun TH, O'Rourke MJ et al (2008) Centrifuge modeling of earthquake effects on buried high-density polyethylene (HDPE) pipelines crossing fault zones. J Geotech Geoenvironmental Eng 134:1501–1515. https://doi.org/10.1061/(asce)1090-0241(2008)134:10(1501)

Halabian AM, Hokmabadi T (2018) A new hybrid model for rigorous analysis of buried pipelines under general faulting accounting for material and geometrical non-linearities with focusing on corrugated HDPE pipelines. Soil Dyn Earthq Eng 115:1–17. https://doi.org/10.1016/j.soildyn.2018.08.005

Jalali HH, Rofooei FR, Attari NKA, Samadian M (2016) Experimental and finite element study of the reverse faulting effects on buried continuous steel gas pipelines. Soil Dyn Earthq Eng 86:1–14. https://doi.org/10.1016/j.soildyn.2016.04.006

Jalali HH, Rofooei FR, Khajeh AAN (2018) Performance of buried gas distribution pipelines subjected to reverse fault movement. J Earthq Eng 22:1068–1091. https://doi.org/10.1080/13632469.2016.1269694

Joshi S, Prashant A, Deb A, Jain SK (2011) Analysis of buried pipelines subjected to reverse fault motion. Soil Dyn Earthq Eng 31:930–940. https://doi.org/10.1016/j.soildyn.2011.02.003

Karamitros DK, Bouckovalas GD, Kouretzis GP (2007) Stress analysis of buried steel pipelines at strike-slip fault crossings. Soil Dyn Earthq Eng 27:200–211. https://doi.org/10.1016/j.soildyn.2006.08.001

Karamitros DK, Bouckovalas GD, Kouretzis GP, Gkesouli V (2011) An analytical method for strength verification of buried steel pipelines at normal fault crossings. Soil Dyn Earthq Eng 31:1452–1464. https://doi.org/10.1016/j.soildyn.2011.05.012

Karamitros DK, Zoupantis C, Bouckovalas GD (2016) Buried pipelines with bends: Analytical verification against permanent ground displacements. Can Geotech J 53:1782–1793. https://doi.org/10.1139/cgj-2016-0060

Kennedy RP, Chow AM, Williamson RA (1977) Fault movement effects on burried oil pipeline. Transp Eng J. https://doi.org/10.1061/tpejan.0000659

Loli M, Kourkoulis R, Gazetas G (2018) Physical and numerical modeling of hybrid foundations to mitigate seismic fault rupture effects. J Geotech Geoenvironmental Eng 144:04018083. https://doi.org/10.1061/(asce)gt.1943-5606.0001966

Loukidis D, Bouckovalas GD, Papadimitriou AG (2009) Analysis of fault rupture propagation through uniform soil cover. Soil Dyn Earthq Eng 29:1389–1404. https://doi.org/10.1016/j.soildyn.2009.04.003

Makrakis N, Psarropoulos PN, Sextos A, Tsompanakis Y (2022a) Quantifying the impact of soft surface soil layers on fault rupture propagation and kinematic distress of offshore and onshore pipelines. 16th Int. Pipeline Tech. Conf. (PTC-2022), Berlin, Germany

Makrakis N, Psarropoulos PN, Sextos A, Tsompanakis Y (2023) New empirical relationships for the assessment of the impact of sandy surface soil deposits on fault rupture propagation. (under review)

Melissianos VE (2022) Onshore buried steel fuel pipelines at Fault Crossings: a review of critical analysis and design aspects. J Pipeline Syst Eng Pract 13:03122002. https://doi.org/10.1061/(ASCE)PS.1949-1204.0000661

Melissianos VE, Korakitis GP, Gantes CJ, Bouckovalas GD (2016) Numerical evaluation of the effectiveness of flexible joints in buried pipelines subjected to strike-slip fault rupture. Soil Dyn Earthq Eng 90:395–410. https://doi.org/10.1016/j.soildyn.2016.09.012

Melissianos VE, Vamvatsikos D, Danciu L, Basili R (2022) An engineering approach to fault displacement hazard for lifelines crossing active tectonic faults. In: 3rd European conference on earthquake engineering, seismology (2022) (3ECEES). Bucharest, Romania

Mortazavi Zanjani M, Soroush A (2019) Numerical modelling of fault rupture propagation through layered sands. Eur J Environ Civ Eng 23:1139–1155. https://doi.org/10.1080/19648189.2017.1344148

Nair GS, Dash SR, Mondal G (2018) Review of pipeline performance during earthquakes since 1906. J Perform Constr Facil 32:04018083. https://doi.org/10.1061/(asce)cf.1943-5509.0001214

Newmark NM, Hall WJ (1975) Pipeline design to resist large fault displacement Proc U.S. Nat Conf Earthq Eng, pp. 416–425

Ng CWW, Cai QP, Hu P (2012) Centrifuge and numerical modeling of normal fault-rupture propagation in clay with and without a preexisting fracture. J Geotech Geoenvironmental Eng 138:1492–1502. https://doi.org/10.1061/(asce)gt.1943-5606.0000719

Ni P, Moore ID, Take WA (2018) Numerical modeling of normal fault-pipeline interaction and comparison with centrifuge tests. Soil Dyn Earthq Eng 105:127–138. https://doi.org/10.1016/j.soildyn.2017.10.011

Nuti C, Rasulo A, Vanzi I (2010) Seismic safety of network structures and infrastructures. Struct Infrastruct Eng 6:95–110. https://doi.org/10.1080/15732470802663813

Özcebe AG, Paolucci R, Mariani S (2017) Numerical modeling of the interaction of pressurized large diameter gas buried pipelines with normal fault ruptures. Soil Dyn Earthq Eng 101:105–115. https://doi.org/10.1016/j.soildyn.2017.07.017

Psyrras N, Gerasimidis S, Kwon O-S, Sextos AG (2018) Can a buried natural gas pipeline buckle locally during earthquake ground shaking? Soil Dyn Earthq Eng 116:511–529. https://doi.org/10.1016/j.soildyn.2018.10.027

Psyrras N, Sextos AG, Crewe A, Dietz M, Mylonakis G (2020) Physical modelling of the seismic response of gas pipelines in laterally inhomogeneous soils. J Geotech Geoenviron Eng. https://doi.org/10.1061/(ASCE)GT.1943-5606.0002242

Robert DJ, Soga K, O'Rourke TD (2016) Pipelines subjected to fault movement in dry and unsaturated soils. Int J Geomech 16:1–16. https://doi.org/10.1061/(asce)gm.1943-5622.0000548

Rofooei FR, Jalali HH, Attari NKA, Alavi M (2012) Full-scale laboratory testing of buried pipelines subjected to permanent ground displacement caused by reverse faulting. Proc 15th World Conf Earthq Eng

Rojhani M, Moradi M, Galandarzadeh A, Takada S (2012) Centrifuge modeling of buried continuous pipelines subjected to reverse faulting. Can Geotech J 49:659–670. https://doi.org/10.1139/T2012-022

Rokonuzzaman M, Nahas AE, Sakai T (2015) Experimental validation of a numerical model for the interaction of dip-slip normal fault ruptures, sand deposits, and raft foundations. Int J Geotech Eng 9:239–250. https://doi.org/10.1179/1939787914Y.0000000057

Saiyar M, Ni P, Take WA, Moore ID (2016) Response of pipelines of differing flexural stiffness to normal faulting. Geotechnique 66:275–286. https://doi.org/10.1680/jgeot.14.P.175

Sarvanis GC, Karamanos SA (2017) Analytical model for the strain analysis of continuous buried pipelines in geohazard areas. Eng Struct 152:57–69. https://doi.org/10.1016/j.engstruct.2017.08.060

Sarvanis GC, Karamanos SA, Vazouras P et al (2018) Permanent earthquake-induced actions in buried pipelines: Numerical modeling and experimental verification. Earthq Eng Struct Dyn 47:966–987. https://doi.org/10.1002/eqe.3001

Scott RF (1987) Fail. Geotechnique 37:423–466

Simulia (2014) Abaqus 6.14. Analysis user's guide. Dassault Systèmes

Taniyama H, Watanabe H (2002) Deformation of sandy deposits by reverse faulting. Struct Eng Earthq Eng 19(2):209s–219s. https://doi.org/10.2208/jsceseee.19.209s

Thebian L, Najjar S, Sadek S, Mabsout M (2018) Numerical investigation of dip-slip fault propagation effects on offshore seabed sediments. Eng Geol 237:149–167. https://doi.org/10.1016/j.enggeo.2018.02.008

Trifonov OV, Cherniy VP (2012) Elastoplastic stress-strain analysis of buried steel pipelines subjected to fault displacements with account for service loads. Soil Dyn Earthq Eng 33:54–62. https://doi.org/10.1016/j.soildyn.2011.10.001

Tsatsis A, Loli M, Gazetas G (2019) Pipeline in dense sand subjected to tectonic deformation from normal or reverse faulting. Soil Dyn Earthq Eng 127:105780. https://doi.org/10.1016/j.soildyn.2019.105780

Turgut A, Isik NS, Kasapoglu KE (2017) A new empirical equation proposed for the relationship between surface rupture length and the earthquake source parameters. Bull Eng Geol Environ 76:383–392. https://doi.org/10.1007/s10064-016-0960-9

Uckan E, Akbas B, Shen J et al (2015) A simplified analysis model for determining the seismic response of buried steel pipes at strike-slip fault crossings. Soil Dyn Earthq Eng 75:55–65. https://doi.org/10.1016/j.soildyn.2015.03.001

Vazouras P, Karamanos SA (2017) Structural behavior of buried pipe bends and their effect on pipeline response in fault crossing areas. Bull Earthq Eng 15:4999–5024. https://doi.org/10.1007/s10518-017-0148-0

Vazouras P, Dakoulas P, Karamanos SA (2015) Pipe-soil interaction and pipeline performance under strike-slip fault movements. Soil Dyn Earthq Eng 72:48–65. https://doi.org/10.1016/j.soildyn.2015.01.014

Wang LR, Yeh Y-H (1985) A refined seismic analysis and design of buried pipeline for fault movement. Earthq Eng Struct Dyn 13:75–96. https://doi.org/10.1002/eqe.4290130109

Wells DL, Coppersmith KJ (1994) New empirical relationships among magnitude, rupture length, rupture width, rupture area, and surface displacement. Bull Seismol Soc Am 84:974–1002

Xie X, Symans MD, O'Rourke MJ et al (2011) Numerical modeling of buried HDPE pipelines subjected to strike-slip faulting. J Earthq Eng 15:1273–1296. https://doi.org/10.1080/13632469.2011.569052

Yoshizaki K, O'Rourke TD, Hamada M (2003) Large scale experiments of buried steel pipelines with elbows subjected to permanent ground deformation. Struct Eng Earthq Eng 20(1):1 s–11 s. https://doi.org/10.2208/jsceseee.20.1s

Zhang L, Zhao X, Yan X, Yang X (2017) Elastoplastic analysis of mechanical response of buried pipelines under strike-slip faults. Int J Geomech 17:04016109. https://doi.org/10.1061/(asce)gm.1943-5622.0000790

Authors and Affiliations

Nikolaos Makrakis[1] · Prodromos N. Psarropoulos[2] · Anastasios Sextos[3] · Yiannis Tsompanakis[1]

Nikolaos Makrakis
nmakrakis@isc.tuc.gr

Prodromos N. Psarropoulos
prod@central.ntua.gr

Anastasios Sextos
a.sextos@bristol.ac.uk

[1] School of Chemical and Environmental Engineering, Technical University of Crete, Sciences Building - Office 141.B.86, University Campus, Chania 731 00, Crete, Greece

[2] School of Rural, Surveying and Geoinformatics Engineering, National Technical University of Athens, Athens, Greece

[3] Department of Civil Engineering, University of Bristol, Bristol, UK